Catalysis Today 146 (2009) 124–131

Contents lists available at ScienceDirect

Catalysis Today

journal homepage: www.elsevier.com/locate/cattod

Rh/MgO/$Ce_{0.5}Zr_{0.5}O_2$ supported catalyst for autothermal reforming of methane: The effects of ceria–zirconia doping

Zhongshan Yuan [a], Changjun Ni [a], Chunxi Zhang [a], Diannan Gao [a], Shudong Wang [a,*], Yuming Xie [b], Akira Okada [b]

[a] Laboratory of Advanced Chemical Engineering, Dalian Institute of Chemical Physics, Chinese Academy of Sciences, No. 457 Rd. Zhongshan, Dalian, 116023, China
[b] Science & Technology, Corning Incorporated, Corning, NY 14831, USA

ARTICLE INFO

Article history:
Available online 1 April 2009

Keywords:
Methane autothermal reforming
Supported Rh/MgO/$Ce_{0.5}Zr_{0.5}O_2$ catalyst
Ceria–zirconia

ABSTRACT

The supported Rh/MgO/$Ce_{0.5}Zr_{0.5}O_2$ catalysts were developed for autothermal reforming of methane. The effects of ceria–zirconia addition on the Rh catalyst were characterized with BET, XRD, SAED, HREM and TPR. The catalytic performance was evaluated on a flow through reactor. Results showed that the addition of ceria–zirconia enhanced the catalyst stability due to the interactions between ceria–zirconia, MgO promoter and the active component Rh. Meanwhile, the selectivity towards hydrogen in reformate was also boosted because of the increased water gas shift activity by the mixed oxides. The results also showed that the structural properties, the textural properties and the redox properties of ceria–zirconia had great influences on the catalyst performance, especially on the catalyst stability. Formations of single phase solid solution, larger pore size as well as Ce/Zr ratio at 1/1 were more desirable for ceria–zirconia dopant. As a result, one of the optimized honeycomb catalysts with the composition of 0.3% Rh/2.5% MgO/43.2% $Ce_{0.5}Zr_{0.5}O_2$/54.0% cordierite (wt.%) has been continually operated at 800 °C up to 2000 h without deactivation.

1. Introduction

Nowadays, worldwide interests in hydrogen energy and fuel cell technologies for a wide range of applications remain very strong. One of the distinct features of the R&D activities is that small stationary/portable fuel cell units have been paid much attention, and there is a growing need for distributed generation of hydrogen via reforming of alcohols, ethers and hydrocarbon fuels for industrial, transportation and residential markets [1–3]. Among the potential fuel sources for hydrogen generation, natural gas (methane) is considered to be one of the preferred fuels since it is clean, abundant, and well-distributed [4]. In the past few years, many natural gas fuel cell systems (so-called combined heat and power system, CHP) have been demonstrated or commercialized for fuel cell stationary/residential applications [5–8].

Options for converting natural gas to hydrogen-rich syngas include three basic processes: steam reforming (SR), partial oxidation (POX) and autothermal reforming (ATR). These technologies are well-established in industrial plant scale and their general differences, advantages and disadvantages have been described well previously [9,10]. Of the above technical routes, ATR is regarded as one of the promising options to provide distributed hydrogen to small stationary/residential fuel cell power systems due to its high efficiency, easy startup, rapid response to power changing and system simplicity [4,11,12]. Newly developed methane ATR technologies combine the two segments of SR and POX into one single compact unit, thus the design of ATR catalysts could be challenging because they have to be robust for both SR and POX reactions, especially in the catalytic zone that runs under limited oxygen. The conventional Ni-based catalysts, e.g., Ni supported on α-Al_2O_3 or $MgAl_2O_4$ [13] seem not suitable for ATR process because they require additional peripheric components and associated units to prevent them from being deactivated by various factors, such as pyrophoric reaction, carbon formation and sulfur poisoning. Perovskite or spinel crystal type of Ni-based catalyst is also apt to sintering upon subject to the redox atmosphere in ATR systems [14]. Therefore, based on the desired performance and compactness of the fuel reformer, platinum group metal (PGM) catalysts tend to be found more preferable in the development of active and stable ATR catalysts. Rh supported on α-Al_2O_3 or other refractory supports have been widely investigated in ATR process [15–17]. However, the insufficiency of the oxidation activity of alumina supported Rh catalyst may lead to the mismatching of the exothermic POX and the endothermic SR processes that occur in ATR reactions, as proposed by Lenz and

* Corresponding author. Tel.: +86 411 84662365; fax: +86 411 84662365.
E-mail address: wangsd@dicp.ac.cn (S. Wang).

0920-5861/$ – see front matter © 2009 Elsevier B.V. All rights reserved.
doi:10.1016/j.cattod.2009.02.032

Aicher [18] and Neumann et al. [19]. Developing bimetallic catalysts might be an effective way to improve the oxidation activity of the catalysts [20,21]. Recently, much effort has been devoted to the modification of the existing ATR catalysts by using promoters having high oxygen storage capacity (OSC), such as the ceria–zirconia mixed oxides. Qi et al. [22] reported that Rh supported on CeO_2 and/or ZrO_2 catalysts were the best candidates for the reforming of hydrocarbons because of their high activity and stability in ATR reaction atmosphere compared to other precious metals and supports. Argonne National Laboratory has also developed a proprietary PGM catalyst supported on mixed oxides such as CeO_2 or $CeGdO_2$ [23]. The improved performance obtained on ceria-containing supports was explained based on the enhancement of the oxygen exchange ability of the catalyst under oxidizing–reducing conditions [24]. However, a lot of work still remains to be done to elucidate the relationship between the property of ceria-based material and the performance of the catalyst. As a matter of fact, the structural properties, textural properties as well as the redox properties of ceria–zirconia mixed oxides play an important role in optimizing the catalyst performance, especially the catalyst stability. Therefore even though the effects of ceria–zirconia addition into the methane ATR catalyst have been widely reported, there is a continuing need for the development of more active and stable supported catalysts for the catalytic conversion of methane to hydrogen.

The aim of the work is to develop an improved Rh/MgO/$Ce_{0.5}Zr_{0.5}O_2$ supported catalyst for methane conversion to hydrogen. The effects of the ceria–zirconia doping on the performance of ATR catalyst were given, and the influences of the structural properties, the textural properties as well as the redox properties of ceria–zirconia mixed oxides were studied and optimized. The performances of the optimized honeycomb catalyst during the long term test and the reaction startup and shutdown cycles were also presented.

2. Experimental

2.1. Catalyst preparation

The pellet catalysts Rh/Al_2O_3, $Rh/Ce_{0.5}Zr_{0.5}O_2/Al_2O_3$ and Rh/MgO/$Ce_{0.5}Zr_{0.5}O_2/Al_2O_3$ were prepared by incipient wetness impregnation with the solution of the corresponding metal precursors of $Ce(NO_3)_3$–$Zr(NO_3)_4$, $Mg(NO_3)_2$ and $RhCl_3$ (Shanghai Chemical Company, China). The catalyst support α-Al_2O_3 was obtained by calcination of γ-Al_2O_3 (Dalian Purtec Chemical Technology Company, China) at 1100 °C for 2 h. After each impregnation, the samples were dried at 120 °C for 10 h and then calcined at 900 °C for 2 h. The weight percent of Rh, MgO and $Ce_{0.5}Zr_{0.5}O_2$ in the catalyst samples were 0.15%, 2.5% and 20% (wt.%, the same hereafter), respectively.

A series of ceramic honeycomb catalysts Rh/MgO/$Ce_xZr_{1-x}O_2$/cordierite (x = 0.80, 0.50 and 0.33) were prepared by ceria–zirconia slurry coating, followed by wet impregnation of $Mg(NO_3)_2$ and $RhCl_3$. The cordierite substrate ($2Al_2O_3{\cdot}2MgO{\cdot}5SiO_2$, Corning Incorporated, USA) was pretreated by 3% HNO_3 solution and then calcinated at 900 °C for 2 h. The ceria–zirconia slurry was obtained by wet ball milling of ceria–zirconia powder prepared by different methods mentioned below. After each preparation procedure, the samples were dried at 120 °C for 3 min in a microwave oven and then calcined at 900 °C for 2 h. The weight percent of Rh, MgO and $Ce_{0.5}Zr_{0.5}O_2$ in the catalyst samples were 0.30%, 2.5% and 43.2%, respectively.

Three preparation methods of $Ce_xZr_{1-x}O_2$ (homogeneous precipitation, coprecipitation and reverse microemulsion, designated as HP, CP and ME, respectively) and two precursors of cerium ($Ce(NO_3)_3{\cdot}6H_2O$ and $(NH_4)_2Ce(NO_3)_6$, Shanghai Chemical Company, China) were selected to investigate the properties of $Ce_xZr_{1-x}O_2$ so as to optimize the catalyst performance [25].

An example of HP method using $(NH_4)_2Ce(NO_3)_6$ as cerium precursor is described below. Amounts of 54.8 g of $(NH_4)_2Ce(NO_3)_6$, 42.9 g of $Zr(NO_3)_4{\cdot}5H_2O$ and 180 g of urea were dissolved in 1500 mL of deionized water, then the aqueous solution was handled by the temperature program up to 100 °C with vigorous stirring until the coprecipitation was observed. The precipitate was then aged at 100 °C for 2 h and washed thoroughly with 1500 mL of deionized water followed by 150 mL of propanol. The resulting filter cake was dried in a vacuum oven at 60 °C for 12 h and calcined at 500 °C for 2 h.

For ME method, 100 mL of NP-10 (polyoxyethylene (10) octyl phenyl alcohol ether) and 120 mL of n-hexyl alcohol were added into 400 mL of cyclohexane with stirring until the mixture became transparent. Then 50 mL of 1 M cerium nitrate solution and 50 mL of 1 M zirconium nitrate solution were added into the above mixture with stirring until it became transparent again. Another microemulsion system which dissolved 100 mL of 12.5% ammonia hydroxide was also prepared under the same procedure described above. Then the two different microemulsion solutions were mixed with vigorous stirring for 0.5 h. The mixture was heated to 70 °C for refluxing 10 min so as to separate the water phase from the oil phase thoroughly. The separated water phase was filtered, dried in a vacuum oven at 70 °C for 12 h followed by calcination at 500 °C for 2 h.

The CP method was also employed for comparison with HP and ME methods. In the CP procedure, 12.5% aqueous ammonia solution was added dropwise into 0.1 M mixed cerium–zirconium nitrate solution under stirring until the pH value reached greater than 9. The precipitate was aged for 2 h and washed thoroughly with deionized water. Then the filter cake was dried in a vacuum oven at 60 °C for 12 h and calcined at 500 °C for 2 h.

2.2. Catalyst characterization

H_2-TPR analysis of the pellet catalysts was conducted in an AutoChem-2920 instrument from 50 °C to 950 °C, at a heating rate of 10 °C/min under a flow of 10 vol% H_2/Ar mixture to examine the interactions between active components and support. The quantitative evaluation of H_2 consumed was done by calibrating the apparatus with the reduction of CuO to metallic copper.

XRD analysis of $Ce_xZr_{1-x}O_2$ powder was carried out on an X'Pert PRO X-ray diffractometer to determine whether a single phase $Ce_xZr_{1-x}O_2$ solid solution was formed.

Specific surface area of $Ce_xZr_{1-x}O_2$ was measured on a nitrogen adsorption volumetric device (NOVA4000 Series) according to the BET method.

High resolution electron microscopy (HREM) images and selected area electron diffraction (SAED) patterns of $Ce_xZr_{1-x}O_2$ powder were recorded with a Phillips Tecnai G220 S-Twin transmission electron microscope operated at an accelerating rate of 200 kV.

2.3. Catalyst performance test

Performance test of catalyst was carried out in a quartz tubular reactor under atmospheric pressure. An amount of 0.5 mL of pellet catalyst with 0.5 mL of inert SiO_2 (0.8–1.0 mm in size)/a piece of honeycomb catalyst (18 mm in height, 52 cells) was charged into the reactor inside an electric furnace. Water was pumped into the evaporator controlled at 200 °C and then mixed with dry feed gas (methane and air) before entering into the reactor. The feed and product gases were analyzed on-line by the GC960 gas chromatograph equipped with a TCD detector and a TDX-01 column (Shanghai Haixin Analytical Instruments, Inc., China). All the

catalysts were reduced in 10 vol% H_2–N_2 gas flow at 700 °C for 2 h prior to reaction in order to avoid the decomposition of Rh_2O_3. All the experiments were performed under the conditions of O_2/methane molar ratio of 0.46, H_2O/methane molar ratio of 2.0 and reaction temperature of 800 °C. Under this experimental conditions, nearly 100% of methane can be converted into reformate. The GHSV of methane was operated at 20,000 h^{-1} for pellet catalysts and 5000 h^{-1} for honeycomb catalysts, respectively.

The following definition was used for describing the catalyst performance:

$$\text{Methane conversion} = \frac{\text{Total mole amount of } (CO + CO_2) \text{ in reformate}}{\text{Total mole amount of feed } CH_4} \times 100\%$$

3. Results and discussion

3.1. Effect of the addition of $Ce_{0.5}Zr_{0.5}O_2$

The methane conversions of different Al_2O_3 supported pellet catalysts as a function of the running time are shown in Fig. 1. It can be seen that although the activity of all the employed catalysts are decreased along with the running time, the catalyst samples with $Ce_{0.5}Zr_{0.5}O_2$ doping are more stable than the comparative sample Rh/Al_2O_3. Data of BET characterization of the fresh catalysts and the aged catalysts listed in Table 1 show that for the aged catalysts, the BET surface areas are very similar within the experimental errors, while the methane conversion at 90 h is obviously different. Taking into account the quite similar initial activity, the enhancement of ceria–zirconia doping can be explained by the formation of the new Rh-oxide species revealed from H_2-TPR behaviors of the corresponding catalysts shown in Fig. 2.

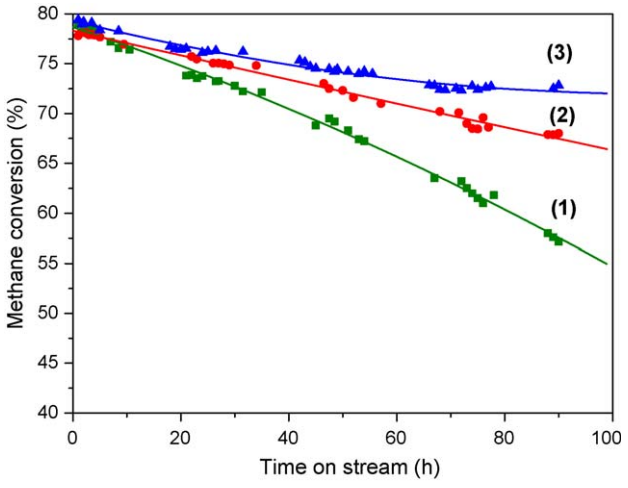

Fig. 1. Methane conversions as a function of the running time over supported pellet catalysts of (1) Rh/Al_2O_3, (2) $Rh/Ce_{0.5}Zr_{0.5}O_2/Al_2O_3$ and (3) $Rh/MgO/Ce_{0.5}Zr_{0.5}O_2/Al_2O_3$.

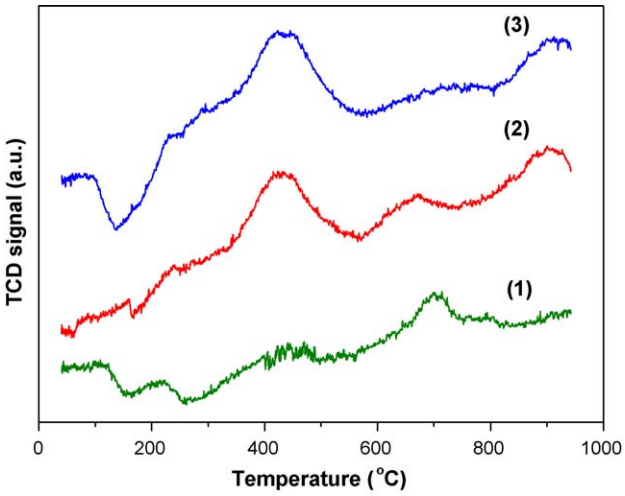

Fig. 2. H_2-TPR profiles of the oxidized supported pellet catalysts of (1) Rh_2O_3/Al_2O_3, (2) $Rh_2O_3/Ce_{0.5}Zr_{0.5}O_2/Al_2O_3$ and (3) $Rh_2O_3/MgO/Ce_{0.5}Zr_{0.5}O_2/Al_2O_3$.

For the TPR profile of Rh_2O_3/Al_2O_3 (trace 1), there is a weak reduction peak of Rh_2O_3 at approximately 200 °C. The very flat TPR peak observed between 250 °C and 550 °C may be due to the various stages of interactions between Rh and Al. A high temperature reduction peak occurs at around 700 °C, and the strong interaction between Al and Rh oxides (especially the formation of $RhAlO_3$) is responsible for the peak [26]. When introducing $Ce_{0.5}Zr_{0.5}O_2$ to the catalyst, the high temperature reduction peak at ca. 700 °C is weakened (trace 2) and further disappears (trace 3), indicating that the strong interaction between Rh and the α-Al_2O_3 support was suppressed. The reduction peaks occur at 900 °C in trace 2 and trace 3 can be associated with the bulk phase reduction of CeO_2, which indicates some inhomogeneity in the Ce–Zr mixed oxides. For the reduction peak of Ce–Zr oxide, it is generally accepted by the researchers [27,28] that when the Ce–Zr oxide was loaded with metal active component, the reduction peak at 450–650 °C shifted towards the low temperature side due to the hydrogen spill-over effect. Therefore, it is reasonable that the wide peak (no formation of a definite compound) occurs at 160–560 °C in trace 2 is attributed to the interaction between Ce–Zr oxide and Rh oxide. And this interaction may be the most important reason responsible for the stability enhancement of the ceria–zirconia doping catalysts (Fig. 1). The new Rh–Ce–Zr–O species can enhance the oxygen mobility of the catalyst due to OSC of $Ce_{0.5}Zr_{0.5}O_2$ material, lead to the better matching of the exothermic methane oxidation and the endothermic MSR reaction during MATR process and thus improve the stability of the catalyst. Besides, it is also beneficial to the stabilization of the tiny Rh crystallites. Accordingly, in the case of trace 3, catalyst stability is further enhanced by the formation of the new interactions of Rh–Mg–Ce–Zr–O and/or Rh–Mg–O (may be the spinel type $MgRh_2O_4$ [29]) in the temperature range of 145–580 °C.

Table 1
Specific surface area, pore volume and pore size of the fresh catalysts and the aged catalysts after 90 h tests.

Catalysts	Surface area ($m^2\ g^{-1}$)	Surface area reduction (%)	Pore volume ($cm^3\ g^{-1}$)	Pore diameter (nm)
Rh/Al_2O_3 (fresh)	57.974		0.201	9.667
Rh/Al_2O_3 (aged)	48.556	16.25	0.176	9.874
$Rh/Ce_{0.5}Zr_{0.5}O_2/Al_2O_3$ (fresh)	55.935		0.195	9.735
$Rh/Ce_{0.5}Zr_{0.5}O_2/Al_2O_3$ (aged)	49.621	11.29	0.173	9.768
$Rh/MgO/Ce_{0.5}Zr_{0.5}O_2/Al_2O_3$ (freash)	52.413		0.164	9.617
$Rh/MgO/Ce_{0.5}Zr_{0.5}O_2/Al_2O_3$ (aged)	47.451	9.47	0.142	9.692

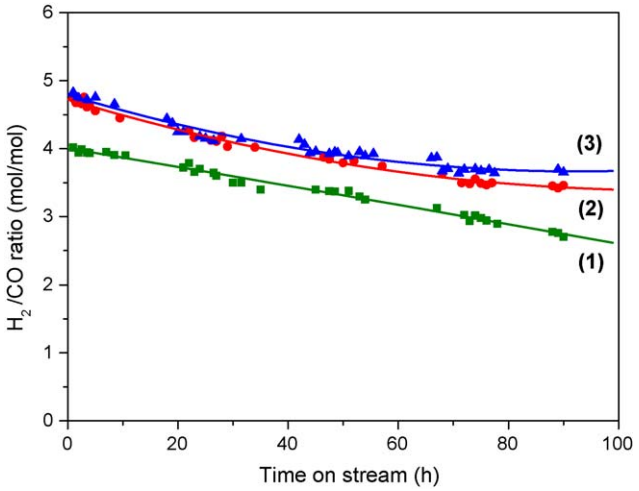

Fig. 3. H_2/CO molar ratio in the reformate gas versus the running time obtained over supported pellet catalysts of (1) Rh/Al_2O_3, (2) $Rh/Ce_{0.5}Zr_{0.5}O_2/Al_2O_3$ and (3) $Rh/MgO/Ce_{0.5}Zr_{0.5}O_2/Al_2O_3$.

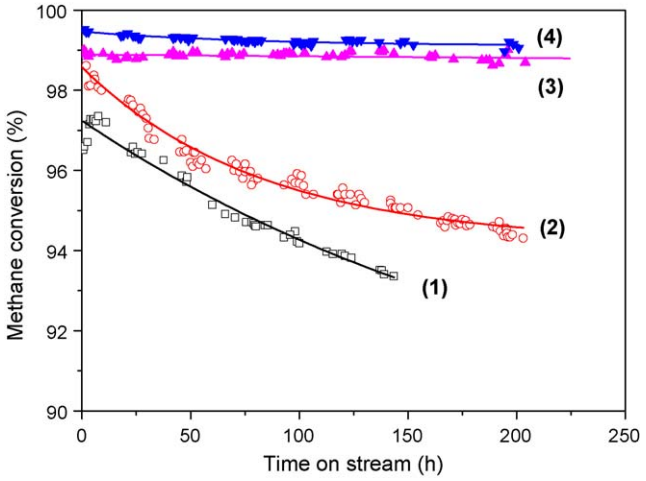

Fig. 4. Methane conversions as a function of the running time over $Rh/MgO/Ce_{0.5}Zr_{0.5}O_2$/cordierite honeycomb catalysts with coated $Ce_{0.5}Zr_{0.5}O_2$ prepared by the methods of (1) homogeneous precipitation using $Ce(NO_3)_3{\cdot}6H_2O$ as precursor (HP/Ce^{3+}), (2) coprecipitation using $Ce(NO_3)_3{\cdot}6H_2O$ as precursor (CP/Ce^{3+}), (3) homogeneous precipitation using $(NH_4)_2Ce(NO_3)_6$ as precursor (HP/Ce^{4+}) and (4) microemulsion using $Ce(NO_3)_3{\cdot}6H_2O$ as precursor (ME/Ce^{3+}).

It is noteworthy that the H_2/CO molar ratio in the reformate product obtained over the ceria–zirconia doping catalysts is significantly higher than that over Al_2O_3 support under the same operating conditions, as shown in Fig. 3. The initial H_2/CO molar ratio obtained over $Rh/Ce_{0.5}Zr_{0.5}O_2/Al_2O_3$ is almost the same compared with that over $Rh/MgO/Ce_{0.5}Zr_{0.5}O_2/Al_2O_3$, this indicates that the increase of H_2/CO molar ratio in the reformate product is solely caused by the addition of ceria–zirconia into the catalyst. Clearly, there presented a promotion towards CO water gas shift (WGS) reaction during ATR process when introducing ceria–zirconia into the catalyst formulations. Similar results have been reported by other researchers [30,31]. Therefore, we suggest that the addition of ceria–zirconia mixed oxides into methane ATR catalyst not only enhance the overall stability of the catalyst, but also provide a potential for reducing CO content in the reformate product thus improving hydrogen output. And this would be further beneficial to the design of the compact fuel processor by reducing the volume of CO WGS reactor.

3.2. Influence of the properties of $Ce_{0.5}Zr_{0.5}O_2$

From the compactness point of view, monolithic catalysts are often employed as alternatives to pellet catalysts for the design of fuel processor due to their high surface to volume ratio and relatively low pressure drop. In the present work, supported ceramic honeycomb catalysts were prepared and examined based on the ceria–zirconia material prepared by different technical routes and ceria precursors. In order to gain nearly full conversion of methane so as to be applied to practical methane ATR processor, more amounts of the active component Rh and the promoter $Ce_{0.5}Zr_{0.5}O_2$ were adopted in the compositions of the supported ceramic honeycomb catalysts. Fig. 4 shows the methane conversions of the supported honeycomb catalysts as a function of the running time. It can be seen from Fig. 4 that the activities of catalysts supported on ceria–zirconia prepared by microemulsion using $Ce(NO_3)_3{\cdot}6H_2O$ as precursor (designated as ME/Ce^{3+}, similarly hereafter) and homogeneous precipitation using $(NH_4)_2Ce(NO_3)_6$ as precursor (HP/Ce^{4+}) are fairly stable during 200 h test, while those supported on ceria–zirconia synthesized through coprecipitation and homogeneous precipitation routes using $Ce(NO_3)_3{\cdot}6H_2O$ as precursors (CP/Ce^{3+} and HP/Ce^{3+}) are gradually decreased along with the running time. Considering the other procedures of the catalyst preparation are all the same, it is believed that the properties of ceria–zirconia, in particular, the structural properties and the redox properties play an important role in catalyst stabilization.

3.2.1. The structural and textural properties of $Ce_{0.5}Zr_{0.5}O_2$

Fig. 5 shows the XRD patterns of the four kinds of ceria–zirconia samples. It can be seen that for the samples of ME/Ce^{3+} and HP/Ce^{4+}, there are four symmetrical reflections in the XRD patterns. No evidence for extra peaks due to non-incorporated ZrO_2 is observed and the slow scanning result of the sample ME/Ce^{3+} confirms the symmetry of the reflections. Compared with the XRD pattern of pure CeO_2 (not shown), the diffraction peaks of these two samples shift to higher degrees, which is attributed to the shrinkage of the lattice due to the replacement of Ce^{4+} (1.09 Å) with a smaller cation radius Zr^{4+} (0.86 Å) [32]. These observations suggest that ZrO_2 is incorporated into the CeO_2 lattice to form a single phase solid solution so as to increase the thermal stability of ceria–zirconia

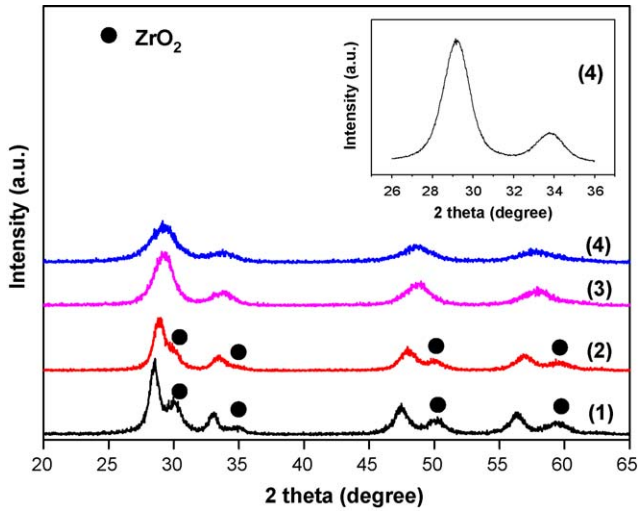

Fig. 5. XRD patterns of ceria–zirconia powders synthesized by (1) homogeneous precipitation using $Ce(NO_3)_3{\cdot}6H_2O$ as precursor (HP/Ce^{3+}), (2) coprecipitation using $Ce(NO_3)_3{\cdot}6H_2O$ as precursor (CP/Ce^{3+}), (3) homogeneous precipitation using $(NH_4)_2Ce(NO_3)_6$ as precursor (HP/Ce^{4+}) and (4) microemulsion using $Ce(NO_3)_3{\cdot}6H_2O$ as precursor (ME/Ce^{3+}). Inset figure presents the slow scanning result of sample (4) at the range of 26–36° 2θ. All samples were calcinated at 500 °C for 2 h.

Table 2
Surface area, pore volume and pore size of the ceria–zirconia samples employed in the present study.

Samples	Ce/Zr molar ratio	Surface area ($m^2\ g^{-1}$)	Pore volume ($cm^3\ g^{-1}$)	Pore diameter (nm)
Homogeneous precipitation using $Ce(NO_3)_3{\cdot}6H_2O$ as precursor (HP/Ce^{3+})	1/1	105.251	0.069	3.383
Coprecipitation using $Ce(NO_3)_3{\cdot}6H_2O$ as precursor (CP/Ce^{3+})	1/1	106.367	0.129	3.806
Homogeneous precipitation using $(NH_4)_2Ce(NO_3)_6$ as precursor (HP/Ce^{4+})	1/1	120.442	0.195	4.571
Microemulsion using $Ce(NO_3)_3{\cdot}6H_2O$ as precursor (ME/Ce^{3+})	1/1	144.212	0.531	9.617
Homogeneous precipitation using $(NH_4)_2Ce(NO_3)_6$ as precursor (HP/Ce^{4+})	4/1	107.223	0.075	3.396
Homogeneous precipitation using $(NH_4)_2Ce(NO_3)_6$ as precursor (HP/Ce^{4+})	1/2	104.407	0.208	5.672

material. However, it is difficult for us to estimate unequivocally the precise phase (cubic or tetragonal) of the solid solution from XRD patterns alone since the composition of $Ce_{0.5}Zr_{0.5}O_2$ was located at the limit of the cubic-tetragonal transition. Contrary to the above samples, in the XRD patterns of the samples of CP/Ce^{3+} and HP/Ce^{3+}, the reflections of ZrO_2 were detected at about 30°, 34°, 50° and 59° 2θ, indicating that a mixture of two phases existed in these two materials. Associated with the performance of different catalysts shown in Fig. 4, it is suggested that ceria–zirconia materials in single phase solid solution are more favourable to the stability of ATR catalyst than those phase-segregated samples.

Textural properties of the employed ceria–zirconia samples were investigated by BET technique. The results are summarized in Table 2 and the pore size distributions of four kinds of samples are presented in Fig. 6. It can be seen that the sample of ME/Ce^{3+} possesses larger pore size and pore volume, compared to the other three samples. Associated with the catalyst performance shown in Fig. 4, it is clear that larger pore volume and pore diameter are beneficial to methane ATR reaction due to its enhanced internal-diffusion. Besides, the higher initial methane conversion occurs on the catalysts supported on ceria–zirconia with larger surface area, and this may be due to the higher dispersion of precious metal of Rh on the ceria–zirconia supports.

The structural and textural properties of the ceria–zirconia samples were further examined by HREM and SAED. Two kinds of samples of ME/Ce^{3+} and HP/Ce^{4+}, which were assured to form the single phase solid solution, were selected and the HREM micrographs and the SAED diffractograms for each sample are collected together in Fig. 7. It can be observed from the SAED diffractograms inset in Fig. 7 that both of the SAED patterns of the two samples show clearly concentric rings and no visible spots at

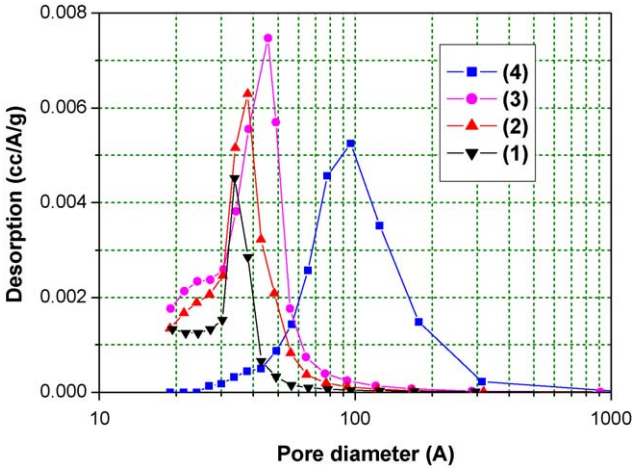

Fig. 6. BJH desorption pore size distributions of ceria–zirconia samples prepared by (1) homogeneous precipitation using $Ce(NO_3)_3{\cdot}6H_2O$ as precursor (HP/Ce^{3+}), (2) coprecipitation using $Ce(NO_3)_3{\cdot}6H_2O$ as precursor (CP/Ce^{3+}), (3) homogeneous precipitation using $(NH_4)_2Ce(NO_3)_6$ as precursor (HP/Ce^{4+}) and (4) microemulsion using $Ce(NO_3)_3{\cdot}6H_2O$ as precursor (ME/Ce^{3+}). All samples were calcinated at 500 °C for 2 h.

the spacing. This confirms the conclusion obtained in XRD characterization that CeO_2 and ZrO_2 are completely incorporated into the single phase solid solution. And these patterns are broadly consistent with a fluorite structure, according to the report of Colón et al. [33]. However, it should be noticed that there are some light spots on the ring bands of the sample of HP/Ce^{4+} which indicates that the tetragonal phases are dominant in the sample of HP/Ce^{4+}. From the HREM micrographs of the two samples, it can be

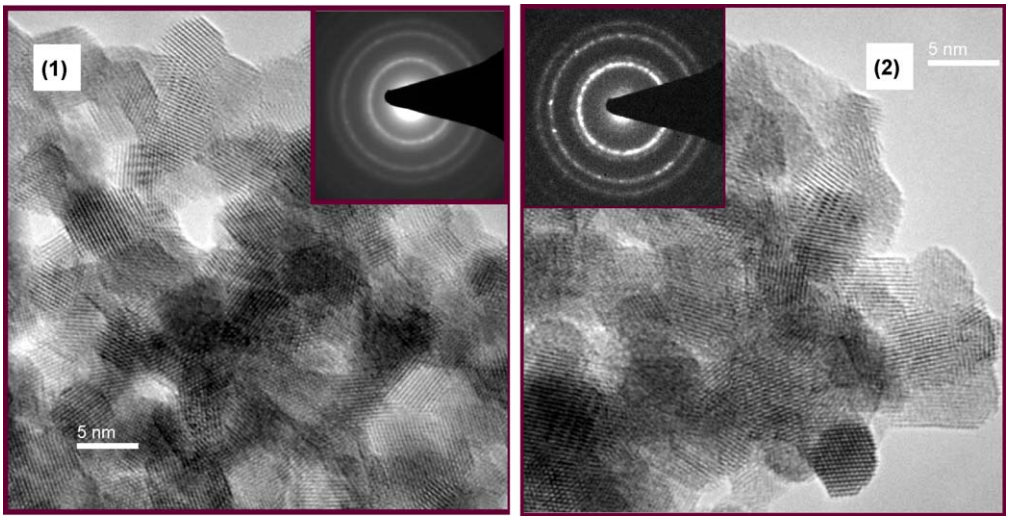

Fig. 7. HREM micrographs and SAED patterns (inset) for $Ce_{0.5}Zr_{0.5}O_2$ prepared by (1) microemulsion using $Ce(NO_3)_3{\cdot}6H_2O$ as precursor (ME/Ce^{3+}) and (2) homogeneous precipitation using $(NH_4)_2Ce(NO_3)_6$ as precursor (HP/Ce^{4+}). Samples were calcinated at 500 °C for 2 h.

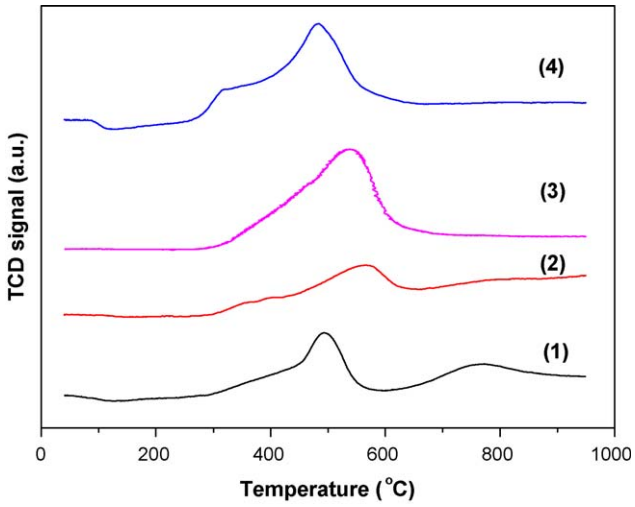

Fig. 8. H_2-TPR profiles of ceria–zirconia materials synthesized by (1) homogeneous precipitation using $Ce(NO_3)_3{\cdot}6H_2O$ as precursor (HP/Ce^{3+}), (2) coprecipitation using $Ce(NO_3)_3{\cdot}6H_2O$ as precursor (CP/Ce^{3+}), (3) homogeneous precipitation using $(NH_4)_2Ce(NO_3)_6$ as precursor (HP/Ce^{4+}) and (4) microemulsion using $Ce(NO_3)_3{\cdot}6H_2O$ as precursor (ME/Ce^{3+}). All samples were calcinated at 500 °C for 2 h.

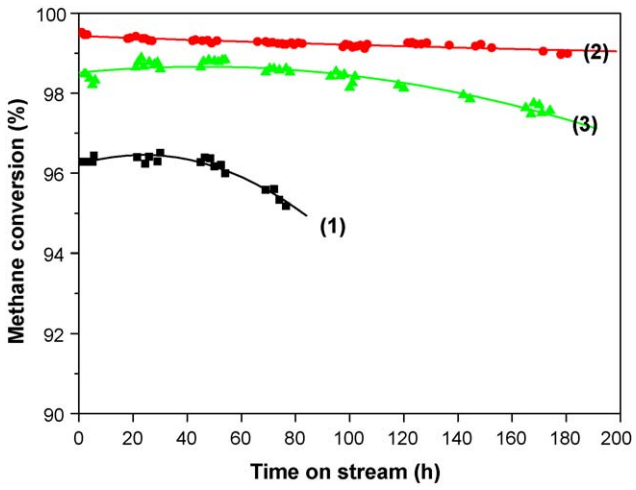

Fig. 9. Methane conversion versus running time over the catalysts supported on $Ce_{0.5}Zr_{0.5}O_2$ with different Ce/Zr molar ratios of (1) 4/1, (2) 1/1 and (3) 1/2. Samples were prepared by homogeneous precipitation using $(NH_4)_2Ce(NO_3)_6$ as precursor (HP/Ce^{4+}).

seen that the bidimensional crystal structure is well-defined. Some pores are found in the micrograph of the sample of ME/Ce^{3+}, which is also in agreement with the results of BET characterization.

3.2.2. The redox behaviors of $Ce_{0.5}Zr_{0.5}O_2$

The TPR profiles of ceria–zirconia prepared by different methods are reported in Fig. 8 and the corresponding H_2 consumptions during TPR process are summarized in Table 3. It can be seen that the redox behaviors of ceria–zirconia strongly depend on the synthesis methods, in other words, the structural and textural properties. The samples of ME/Ce^{3+} and HP/Ce^{4+} show essentially a broad and intensive reduction feature centering around 490 °C and 540 °C, respectively. The observed asymmetry indicates that the broad reduction feature is coupled of two overlapped peaks, which can be attributed to the reduction of the surface and bulk phases of ceria–zirconia, respectively. In fact, a shoulder at around 330 °C is already seen in the case of ME/Ce^{3+}. In contrast, the samples of CP/Ce^{3+} and HP/Ce^{3+} present two separate reduction features, corresponding to the surface and the bulk reduction of the samples. The distinguished bulk reduction peak occurs at high temperature can be associated with the sample inhomogeneity and this confirms the results obtained in XRD analysis. Apparently, the bulk reduction peaks of the samples of ME/Ce^{3+} and HP/Ce^{4+} shift to lower temperature range compared to those of CP/Ce^{3+} and HP/Ce^{3+}. This suggests that the redox behavior of ceria–zirconia is improved when CeO_2 and ZrO_2 form into a single phase solid solution. Furthermore, the H_2 consumptions of ME/Ce^{3+} and HP/Ce^{4+} during TPR experiments are also higher than those of CP/Ce^{3+} and HP/Ce^{3+} (Table 3). Therefore, there is clear evidence that the complete solubility in ceria–zirconia binary system not only provides better thermal resistance during high temperature use, but also enhances the OSC of the material and thus exhibits better redox behavior in reactions.

3.3. Influence of the Ce/Zr molar ratio in $Ce_xZr_{1-x}O_2$

The methane conversions versus running time over the catalysts supported on $Ce_{0.5}Zr_{0.5}O_2$ with different Ce/Zr molar ratios are shown in Fig. 9. It can be seen that the catalyst sample with Ce/Zr molar ratio at 1/1 shows higher methane conversion and better stability than those at 4/1 and 1/2. This suggests that the Ce/Zr molar ratio is also a crucial factor for the chemical behavior of ceria–zirconia material. Results of BET, XRD and H_2-TPR characterization of ceria–zirconia with different Ce/Zr ratios are reported in Table 2, Figs. 10 and 11, respectively. Besides the straightforward correlations between methane conversions and the surface areas of different ceria–zirconia materials, different catalyst stabilities can be associated with XRD patterns and H_2-TPR behaviors of ceria–zirconia.

XRD patterns shown in Fig. 10 reveal that the formation of a homogeneous solid solution has been achieved in all the three samples. Compared to the reflections of $Ce_{0.5}Zr_{0.5}O_2$, there is a left shift of the reflections of $Ce_{0.8}Zr_{0.2}O_2$, e.g., from 29.5° 2θ observed for $Ce_{0.5}Zr_{0.5}O_2$ to 28.8° 2θ observed for $Ce_{0.8}Zr_{0.2}O_2$, which indicates that $Ce_{0.8}Zr_{0.2}O_2$ presents a cubic-fluorite phase structure. In contrast, tetragonal phase structure is observed for the sample $Ce_{0.33}Zr_{0.67}O_2$. An investigation of the effects of ZrO_2 content on the thermal stability of ceria–zirconia suggests that the ZrO_2-rich compositions are more thermally stable compared to CeO_2-rich

Table 3
H_2 consumptions during H_2-TPR experiments of the ceria–zirconia samples employed in the present study.

Samples	Ce/Zr molar ratio	H_2 consumptions (μmol)		H_2 consumptions (μmolg^{-1})
		Around 300–600 °C	Around 600–900 °C	Total
Homogeneous precipitation using $Ce(NO_3)_3{\cdot}6H_2O$ as precursor (HP/Ce^{3+})	1/1	30.309	16.455	467.634
Coprecipitation using $Ce(NO_3)_3{\cdot}6H_2O$ as precursor (CP/Ce^{3+})	1/1	33.185	9.096	422.805
Homogeneous precipitation using $(NH_4)_2Ce(NO_3)_6$ as precursor (HP/Ce^{4+})	1/1	81.073	–	810.733
Microemulsion using $Ce(NO_3)_3{\cdot}6H_2O$ as precursor (ME/Ce^{3+})	1/1	79.930	–	799.296
Homogeneous precipitation using $(NH_4)_2Ce(NO_3)_6$ as precursor (HP/Ce^{4+})	4/1	60.984	3.721	647.053
Homogeneous precipitation using $(NH_4)_2Ce(NO_3)_6$ as precursor (HP/Ce^{4+})	1/2	66.399	–	663.991

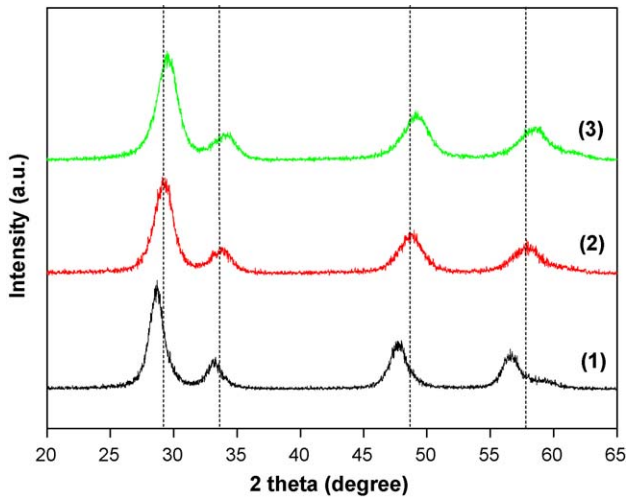

Fig. 10. XRD patterns of ceria–zirconia powders with different Ce/Zr molar ratios of (1) 4/1, (2) 1/1 and (3) 1/2. Samples were prepared by homogeneous precipitation using $(NH_4)_2Ce(NO_3)_6$ as precursor (HP/Ce^{4+}) and were calcinated at 500 °C for 2 h.

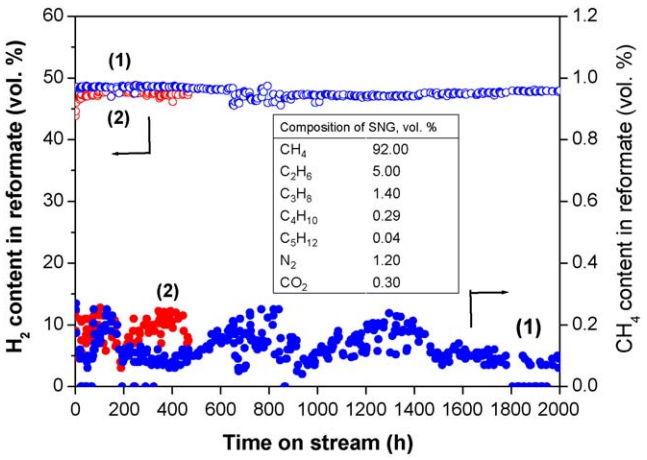

Fig. 12. Long term tests of the optimized honeycomb catalyst (0.3% Rh/2.5% MgO/43.2% $Ce_{0.5}Zr_{0.5}O_2$/54.0% cordierite) in (1) pure methane and (2) simulated natural gas (SNG). Inset table presents the composition of SNG.

compositions [34]. The results of our study are consistent with the fact. Results shown in Fig. 9 indicate that the ZrO_2-rich solid solution in tetragonal phase favors for catalyst stability more than the CeO_2-rich composition in cubic-fluorite phase.

The importance of Ce/Zr molar ratio in ceria–zirconia material can be further illuminated by H_2-TPR profiles. It can be seen from Fig. 11 that the single reduction peak of $Ce_{0.5}Zr_{0.5}O_2$ centers around 540 °C and ends at 740 °C, while the peak reduction temperature of $Ce_{0.33}Zr_{0.67}O_2$ occurs at 560 °C. An additional reduction peak at around 810 °C of $Ce_{0.8}Zr_{0.2}O_2$ indicates that it is hard to be reduced at lower temperatures. It should be mentioned that no decrease of the reduction temperature is observed for higher Ce content sample of $Ce_{0.8}Zr_{0.2}O_2$. This is contrary to the results of Trovarelli et al. [35] but consistent with that of Fornasiero et al. [27], and the effect may depend on the preparation conditions of ceria–zirconia and the experimental conditions. The lower reduction temperature as well as higher H_2 consumption (see Table 3) suggests that $Ce_{0.5}Zr_{0.5}O_2$ has better redox behavior compared to the other two samples. And this, according to the previous discussions, is believed to be beneficial to methane ATR catalyst.

3.4. Stability tests of the optimized catalysts

Based on the fundamental understanding of the current catalyst system, one of the optimized honeycomb catalyst with the composition of 0.33% Rh/2.52% MgO/43.2% $Ce_{0.5}Zr_{0.5}O_2$/54.0% cordierite, of which $Ce_{0.5}Zr_{0.5}O_2$ was prepared by HP/Ce^{4+}, was continuously tested for over 2000 h. The operating conditions were set at O_2/methane molar ratio of 0.46, H_2O/methane molar ratio of 2.0, GHSV of methane of 5000 h^{-1} and reaction temperature of 800 °C, respectively. Results are shown in curve 1 in Fig. 12. It can be seen that the residual methane in the reformate gas is less than 0.25 vol% during the long term test, which means more than 99.0% of methane have been consistently converted into syngas with constant H_2 output. Similar result was also obtained in 500 h test of which the simulated natural gas (SNG) was employed as the reactant. The SNG contained extra C2–C5 compounds (the compositions are shown in table inset in Fig. 12), which may lead to catalyst deactivation by carbon formation during reforming reaction. But even with this possible condition, the ATR catalyst maintains sufficient catalytic activity over the duration of this study, as observed in curve 2 in Fig. 12. This result implies that the methane ATR catalyst developed in

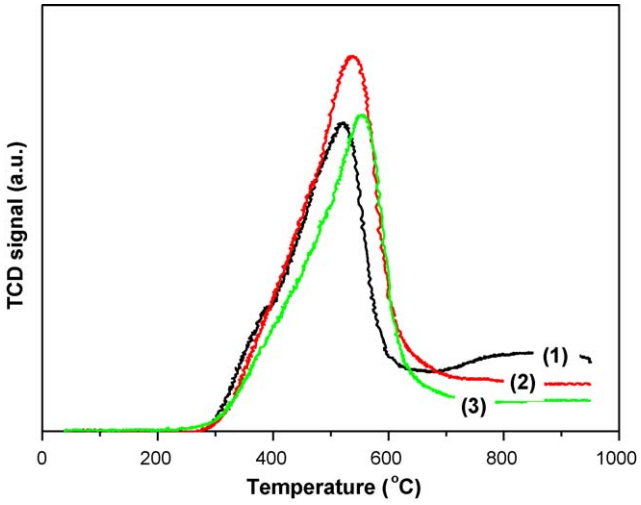

Fig. 11. H_2-TPR profiles of $Ce_{0.5}Zr_{0.5}O_2$ with the Ce/Zr molar ratios of (1) 4/1, (2) 1/1 and (3) 1/2. Samples were prepared by homogeneous precipitation using $(NH_4)_2Ce(NO_3)_6$ as precursor (HP/Ce^{4+}) and were calcinated at 500 °C for 2 h.

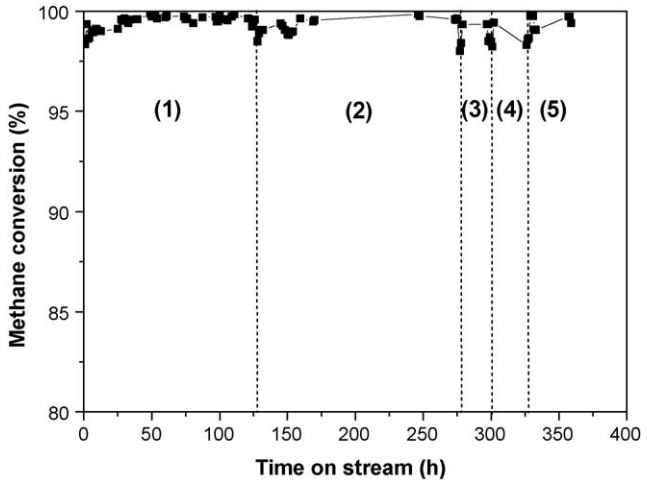

Fig. 13. Transient performance of the optimized honeycomb catalyst (0.3% Rh/2.5% MgO/43.2% $Ce_{0.5}Zr_{0.5}O_2$/54.0% cordierite) during five times of startup and shutdown cycles.

this study may also be suitable for the reforming of other heavy hydrocarbons.

Another desirable characteristic of ATR catalysts for distributed hydrogen production is the resistance to intermittent operations, particularly the cycles of startup and shutdown. We further explored the ability of the optimized honeycomb catalyst to retain activity over the multiple startup/shutdown cycles. Five turns of startup and shutdown were undergone, as shown in Fig. 13. Almost no deactivation is observed over the catalyst during the intermittent operation, thus ensuring that the catalyst of the present work is applicable to the methane ATR fuel processor to provide hydrogen to fuel cell under non-steady operation conditions.

4. Conclusions

With mixed ceria–zirconia doping, the interactions between ceria–zirconia and the active component Rh could improve the oxygen exchange ability of the catalyst and thus lead to the enhancement of the overall performance of the Rh-based methane ATR catalyst. Simultaneously, the H_2/CO molar ratio in the reformate product could also increased due to the increased CO WGS activity.

It is demonstrated in the present work that the structural properties, together with the textural properties and redox properties of ceria–zirconia greatly affect the catalysts performance. Compared with the phase-segregated samples synthesized through coprecipitation (Ce^{3+} as precursor, similarly hereafter) and homogeneous precipitation (Ce^{3+}) route, CeO_2–ZrO_2 prepared by microemulsion (Ce^{3+}) or homogeneous precipitation (Ce^{4+}) can form fine single phase solid solution with larger pore size, which are more favourable for catalyst stability. Further, it is suggested that for Ce/Zr molar ratio, 1/1 is the good choice resulting stable phase structure and better redox property.

The optimized honeycomb catalyst at the composition of 0.33% Rh/2.52% MgO/43.2% $Ce_{0.5}Zr_{0.5}O_2$/54.0% cordierite, of which $Ce_{0.5}Zr_{0.5}O_2$ was prepared by HP/Ce^{4+}, was tested for 2000 h test in pure methane and 500 h test in simulated natural gas. In both cases, more than 99.0% of conversion was obtained under the present operating conditions. Methane conversion also kept constant during five turns of startup and shutdown operation. It is concluded that the optimized catalyst can be a promising candidate for the distributed H_2 production via methane ATR process.

Acknowledgements

The authors gratefully acknowledge the support of Corning Incorporated (USA) under the Joint Research Master Agreement between Dalian Institute of Chemical Physics (China) and Corning Incorporated (USA). Part of the present work was subsidized by the National Basic Research Program of China (No. 2004CB719506) and the National High Technology Research and Development Program of China (No. 2007AA05Z148). The authors also appreciate Dr. Tianjun Sun and Dr. Lei Cao for their kindly help in the analysis of HREM micrographs.

References

[1] G. Kolb, J. Schürer, D. Tiemann, M. Wichert, R. Zapf, V. Hessel, H. Löwe, J. Power Sources 171 (2007) 198.
[2] T. Giroux, S. Hwang, Y. Liu, W. Ruettinger, L. Shore, Appl. Catal. B 56 (2005) 95.
[3] C. Song, Catal. Today 77 (2002) 17.
[4] S.H.D. Lee, D.V. Applegate, S. Ahmed, S.G. Calderone, T.L. Harvey, Int. J. Hydrogen Energy 30 (2005) 829.
[5] O. Okada, K. Yokoyama, Fuel Cells 1 (2001) 72.
[6] D. Sioue, D. Cepla, K. Doshi, J. Harness, Fuel Cell Seminar Abstracts, 2002, p. 772.
[7] N.M. Sammes, R. Boersma, J. Power Sources 86 (2000) 98.
[8] C. Bentley, M. Farooque, H. Maru, J. Leitman, Fuel Cell Seminar Abstracts, 2000, p. 456.
[9] J.N. Armor, Appl. Catal. A 176 (1999) 159.
[10] S.S. Bharadwaj, L.D. Schmidt, Fuel Process. Technol. 42 (1995) 109.
[11] S. Ayabe, H. Omoto, T. Utaka, R. Kikuchi, K. Sasaki, Y. Teraoka, K. Eguchi, Appl. Catal. A 241 (2003) 261.
[12] A. Docter, A. Lamm, J. Power Sources 84 (1999) 194.
[13] J. Zhang, Y. Wang, R. Ma, D. Wu, Appl. Catal. A 243 (2003) 251.
[14] A. Qi, S. Wang, G. Fu, C. Ni, D. Wu, Appl. Catal. A 281 (2005) 233.
[15] B. Li, K. Maruyama, M. Nurunnabi, K. Kunimori, K. Tomishige, Appl. Catal. A 275 (2004) 157.
[16] O.V. Buyevskaya, K. Walter, D. Wolf, M. Baerns, Catal. Lett. 38 (1996) 81.
[17] I. Aartun, B. Silberova, H. Venvik, P. Pfeifer, O. Görke, K. Schubert, A. Holmen, Catal. Today 105 (2005) 469.
[18] B. Lenz, T. Aicher, J. Power Sources 149 (2005) 44.
[19] D. Neumann, M. Kirchhoff, G. Veser, Catal. Today 98 (2004) 565.
[20] B.S. Caglayan, A.K. Avci, Z.İ. Önsan, A.E. Aksoylu, Appl. Catal. A 280 (2005) 181.
[21] S. Freni, G. Calogero, S. Cavallaro, J. Power Sources 87 (2000) 28.
[22] A. Qi, S. Wang, C. Ni, D. Wu, Int. J. Hydrogen Energy 32 (2007) 981.
[23] S.H. Chan, H.M. Wang, J. Power Sources 101 (2001) 188.
[24] G.B. Hoflund, S.D. Gardner, D.R. Schryer, B.T. Upchurch, E.J. Kielen, React. Kinet. Catal. Lett. 58 (1996) 19.
[25] S. Wang, Z. Yuan, C. Ni, Y. Xie, A. Okada, Chinese Patent 200710106098.9 (2007).
[26] P. Fornasiero, R. Di Monte, G. Ranga Rao, J. Kašpar, S. Meriani, A. Trovarelli, M. Graziani, J. Catal. 151 (1995) 168.
[27] H.C. Yao, Y.F. Yu Yao, J. Catal. 86 (1984) 254.
[28] A. Trovarelli, G. Dolcetti, C. de Leitenburg, J. Kašpar, P. Finetti, A. Santoni, J. Chem. Soc., Faraday Trans. 88 (1992) 1311.
[29] E. Ruckenstein, H.Y. Wang, Appl. Catal. A 198 (2000) 33.
[30] X. Wu, L. Xu, D. Weng, Appl. Surf. Sci. 221 (2004) 375.
[31] N. Laosiripojana, S. Assabumrungrat, Appl. Catal. A 290 (2005) 200.
[32] K. Otsuka, W. Ye, M. Nakamura, Appl. Catal. A 183 (1999) 317.
[33] G. Colón, F. Valdivieso, M. Pijolat, R.T. Baker, J.J. Calvino, S. Bernal, Catal. Today 50 (1999) 271.
[34] R. Di Monte, J. Kašpar, J. Mater. Chem. 15 (2005) 633.
[35] A. Trovarelli, F. Zamar, J. Lorca, C. de Leitenburg, G. Dolcetti, J.T. Kiss, J. Catal. 169 (1997) 490.